Physics of Fluids

On the use of leading-edge serrations for noise control in a tandem airfoil configuration

Cite as: Phys. Fluids **32**, 077102 (2020); https://doi.org/10.1063/5.0012958
Submitted: 06 May 2020 . Accepted: 10 June 2020 . Published Online: 01 July 2020

SH. S. Vemuri, X. Liu, B. Zang, and M. Azarpeyvand

Physics of Fluids ARTICLE scitation.org/journal/phf

On the use of leading-edge serrations for noise control in a tandem airfoil configuration

Cite as: Phys. Fluids 32, 077102 (2020); doi: 10.1063/5.0012958
Submitted: 6 May 2020 • Accepted: 10 June 2020 •
Published Online: 1 July 2020

SH. S. Vemuri,[a] X. Liu, B. Zang, and M. Azarpeyvand[b]

AFFILIATIONS

Faculty of Engineering, University of Bristol, Bristol BS8 1TR, United Kingdom

[a]**Author to whom correspondence should be addressed:** shsvemuri@gmail.com and hari.vemuri@bristol.ac.uk
[b]**Electronic mail:** m.azarpeyvand@bristol.ac.uk

ABSTRACT

Passive noise control for a tandem NACA 65-710 airfoil configuration is experimentally investigated by applying leading-edge serrations on the rear airfoil. With a sliding side-plate mechanism that allows the rear airfoil to move in the vertical direction relative to the front airfoil, the position of maximum turbulence interaction noise is first identified from the far-field noise measurements. Subsequently, detailed static surface pressure distribution and unsteady surface pressure fluctuations are acquired to shed more light on the physical phenomenon and underlying noise-reduction mechanism of the leading-edge serrations. The far-field noise measurements confirm that a notable turbulence interaction noise reduction can be achieved from 600 Hz $< f <$ 3000 Hz, agreeing well with the previous literature on the effectiveness of the leading-edge serrations. The near-field hydrodynamic analyses obtained using remote-sensing techniques of the fluctuating pressure fields over the airfoil show that a significant reduction in the surface pressure fluctuation levels up to 20 dB/Hz can be observed at the serrated-tip plane of the rear serrated airfoil close to the leading-edge regions, over the range of frequencies investigated. Although reduction can also be observed on the serrated-root plane, the magnitude is much less significant. The present results suggest that the modification of the unsteady loading on the rear airfoil by the leading-edge serrations plays a crucial role in the reduction of turbulence interaction noise in the tandem airfoil configuration, which may find practical application for noise reduction in aerodynamic systems involving rows of airfoils, such as contra-rotating open rotors and outlet guide vanes.

I. INTRODUCTION

The noise arising from rotating aero-components in several engineering applications such as aviation, turbo-machinery, and wind turbines remains a major concern to date.[1] The negative impact of the exposure to such noise sources, experienced in its full severity especially by people living in close proximity to airports and wind turbines, is undisputable. As a result, increasingly stringent restrictions on noise generation are being imposed on the aviation industry in general, and tremendous research efforts are being dedicated to reducing such noise in the past few decades.

In the case of airfoils, the aerodynamic noise generation occurs due to either airfoil self-noise or turbulence interaction noise.[2] The former arises from the airfoil interacting with its own turbulent boundary layer, while the latter arises due to the incoming free-stream turbulence interacting with the leading edge of the airfoil. It is well-known that the trailing-edge noise, which occurs when the pressure fluctuation from its surface is scattered by the trailing-edge boundary, forms a major component of airfoil self-noise. It is possible to control the trailing-edge noise by passive means, such as changing its surface geometry, or by active means, which generally work by modification of the flow structure in a desirable way over its surface. A range of techniques, such as the use of trailing-edge serrations,[3] fitting trailing-edge brushes,[4] use of porous treatments,[5] morphing,[6] flow suction,[7] and injection,[8] have been shown to be effective for reducing trailing-edge noise at source.

The introduction of increased bypass-ratio turbofan engines has resulted in a significant reduction of jet noise, and the broadband noise arising from the fan now contributes to the majority of the noise generated by aircraft engines. A significant contribution of the fan noise arises from the rotor–stator interaction noise, i.e., the upstream rotor-wake turbulence interacting with the leading edge

of the downstream outlet guide vanes (OGVs). It is hypothesized that the noise generation mechanism of the leading-edge turbulence interaction noise is due to the approaching pressure fluctuations leading to the formation of a fluctuating pressure-dipole source on the surface of the leading edge, with a strength directly proportional to the fluctuating force component acting normal to the surface.[9] This turbulence interaction noise can potentially become the dominating source when the leading edge confronts with sufficiently high levels of incoming turbulence.[10] As a result, significant research efforts have also been expended to understand and propose strategies for turbulence interaction noise reduction. Among them, one of the promising ideas involves the use of leading-edge serrations. Attempts to suppress turbulence interaction noise using serrated leading edges were initially inspired by nature: for instance, humpback whales have shown better hydrodynamic performance due to their serrated flippers[11] and owls are known to be quieter than pigeons due to serrations on their wings.[12] It is shown by various recent research that the application of leading-edge serrations can reduce the turbulence interaction noise significantly with a small loss of aerodynamic performance in pre-stall conditions while also being able to produce a more gradual stall and enhanced post-stall aerodynamic performance.[13] In cases where aerodynamic performance is not of greatest concern, such as in the context of OGVs, the application of leading-edge serrations could prove highly valuable.

Indeed, early efforts by Soderman[14] demonstrated noise reduction with the use of leading-edge serration by carrying out a comparative study of noise characteristics for rotors with serrated leading edges by varying serration geometries, rotor diameters, rotor speeds, and angles of attack. Hersh *et al.*[15] explained the noise-reduction mechanism by studying leading-edge serrations on stationary and rotating airfoils. They showed that the application of serration results in vortices that alter the structure of any periodic velocity fluctuations downstream to random ones, resulting in noise reduction. In the recent years, a lot of work has been devoted to studying noise reduction achieved by single-wavelength, sinusoidal leading-edge serrations, optimization of their serration-geometry parameters and inlet conditions to achieve the best noise reduction, and identification of the key non-dimensional parameters and their dependence on the achieved noise reduction.[16–25] More recently, the idea has been extended to using double-wavelength serrations[26] and more sophisticated serration geometries[27,28] such as chopped-peak and slitted-root, which are shown to provide enhanced noise reduction than the single-wavelength serrations.

The noise-reduction mechanism of the use of serrations has been studied extensively, analytically,[22] numerically,[18,21] and experimentally.[19,20,29] The serrated leading edges induce an unsynchronized response in span, resulting in smaller amplitudes and derivatives of surface pressure fluctuations along the span.[26,30,31] The magnitude of the propagated sound is directly proportional to the unsteady loading at the source location (Ffowcs Williams–Hawkings equation[30]), and therefore, the reduction in unsteady surface pressure locally leads to a global reduction, resulting in lower radiated far-field noise. The mechanism for the single-wavelength serrations, sometimes also referred to as the "source cut-off effect,"[18] involves the reduction of the dipole source strength along the entire span of the leading edge except along the root location. The source strength at the root location (which is fundamentally different from the tip location) remains similar to that of a baseline airfoil (i.e., the one with the straight leading edge) of similar geometry.[28]

As the above review shows, most of the literature available to date on leading-edge serrations and the underlying noise-reduction mechanism focusses on using single airfoils with various serration approaches, whereas studies on interaction noise from a tandem airfoil configuration, i.e., two airfoils arranged in tandem, remain quite limited. Gruber *et al.*[32] investigated the use of combined trailing-edge and leading-edge serrations in a tandem airfoil configuration. They concluded that the combination produced notable noise reduction across a broadband frequency range and attempted to quantify the individual noise-reduction contributions from leading- and trailing-edge serrations applied on the rear and the front airfoils, respectively. To study possible noise reduction and its underlying mechanisms as well as to provide valuable experimental data on the turbulence interaction noise of tandem airfoils, the present work focusses on applying leading-edge serrations to the rear airfoil in a tandem configuration as a passive control strategy, which aims to put the leading-edge serration technology in a better engineering perspective and to help better understand the near-field flow dynamics and far-field noise characteristics of the serrated leading-edge applications. In the tandem configurations tested, the rear airfoil is subjected to a turbulent-flow field generated by the front airfoil, and therefore, the dominant noise source is supposed to be due to the turbulence interaction.

In a preliminary parametric study on the application of leading-edge serrations for tandem airfoil configurations,[34] far-field noise reduction was observed for different airfoil gap distances (W_x) and angles of attack (α). The overall noise reduction achieved at a given streamwise gap distance (W_x) was, however, seen to depend on various other parameters, such as the angle of incidence (α), the vertical location (W_y) of the rear airfoil, and the flow conditions, as shown in Fig. 2. Building on this parametric study, experiments in the present study have been completely redone for one specific case to obtain a detailed hydrodynamic and aeroacoustic study, with the objectives to better understand the underlying physics of the noise-reduction mechanism.

A thorough experimental investigation has been carried out in the present study to assess the noise-suppression effectiveness of leading-edge serrations on the rear airfoil in a tandem airfoil configuration. The layout of this paper is as follows. Section II explains the experimental setup: the aeroacoustic facility, the test rig, and the measurement approach (pressure, far-field and near-field). The results and discussion are presented in Sec. III, where far-field noise and steady and unsteady surface pressure measurements are presented and results are analyzed. This is followed by conclusions and some ideas for future work.

II. EXPERIMENTAL SETUP

A. Experimental facility

The experiments are performed at the University of Bristol Aeroacoustic Facility, which is a closed-circuit type open-jet anechoic wind tunnel. The aeroacoustic facility comprises of a large anechoic chamber ($7.9 \times 5.0 \times 4.6$ m^3), fully anechoic from frequencies above 160 Hz, and a temperature-controlled closed-circuit wind

tunnel with an open test section. A 500 × 775 mm^2 rectangular nozzle with a contraction ratio of 8.4:1 is used in this work that has a low turbulence intensity of ~0.2% and high flow quality and uniformity. The tunnel with this nozzle can achieve a maximum speed of 45 m/s. More details of the experimental facility, including its design, dimensions, and flow characteristics, can be found in Ref. 33.

B. Airfoils and serrations

The present experimental study investigates the effectiveness of leading-edge serrations applied to the rear airfoil in a tandem airfoil configuration in reducing the radiated far-field noise from the tandem arrangement. Furthermore, by using instrumentation on the rear airfoils, this study provides a detailed comparison of the aerodynamic and the aeroacoustic performance of the rear serrated and rear baseline, i.e., straight leading edge, airfoils in tandem arrangement. Figure 1 shows a schematic of the experimental setup. Two NACA 65-710 airfoils are mounted in a tandem configuration, i.e., one behind another with reference to the free-stream direction, to a set of side plates, laser-cut precisely to fit the nozzle dimensions. The airfoils are aligned in the center of the nozzle, ~305 mm downstream of the nozzle exit plane, such that both airfoils stay within the potential core of the jet. The side plates are held in place attached to a structure assembly made of aluminum struts, which is then mounted firmly onto the nozzle to minimize any flow-induced vibration and noise. Both the front and rear airfoils are of the chord length c = 150 mm. This choice of the chord length ensures that the entire tandem airfoil setup stays within the potential core of the exiting jet.[33] The alignment of the rectangular side plates to the nozzle helps maintain a nearly two-dimensional flow over the airfoils. The front airfoil has been tripped with a zigzag turbulator on both pressure and suction sides at 14% chord (21 mm) from the leading edge to induce bypass transition to turbulence on both sides and avoid tonal noise due to Tollmien–Schlichting instabilities interacting with the trailing edge. All measurements have been taken at a free-stream velocity of U_0 = 25 m/s, which corresponds to a chord-based Reynolds number of $Re_c \approx 2.5 \times 10^5$.

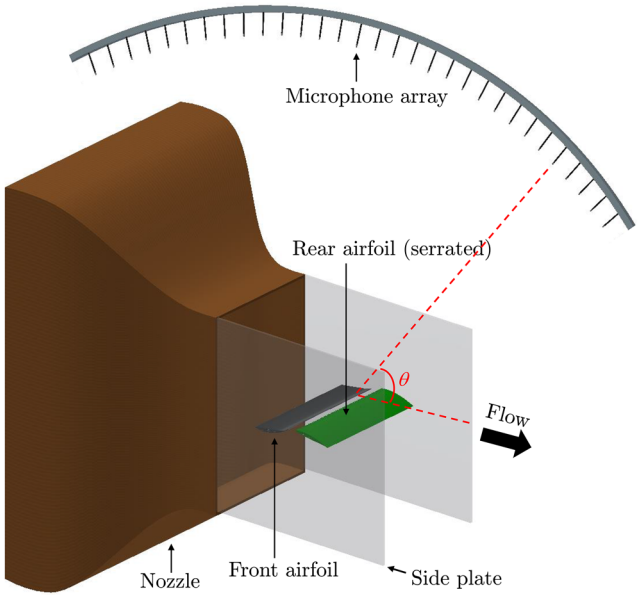

FIG. 1. Schematic description of the tandem airfoil configuration and the microphone array.

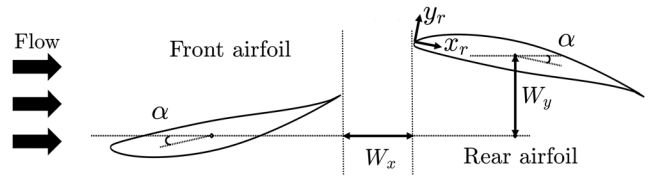

FIG. 2. A schematic showing the tandem-configuration parameters, the angle of incidence (α) and the flow direction.

Figure 2 shows the side-view of the tandem airfoil configuration, along with the important parameters and coordinate systems defining the tandem arrangements. The gap distances W_x and W_y are used to define the relative location of the two airfoils in the streamwise and vertical directions, respectively. Having tested the general capability of the present passive control technique for various other W_x values in an earlier parametric study,[34] only one of the cases, i.e., $W_x = 0.3c$, is chosen to focus our attention fully on the underlying mechanism leading to the reduction of noise when leading-edge serrations are applied in the tandem airfoil configurations. In the present experiments, while the streamwise gap distance between the airfoils W_x is kept constant at $0.3c$, the vertical gap distance W_y is varied systematically to fully capture the wake of the front airfoil. Note that $W_y = 0$ corresponds to the centers of the front and rear airfoils aligned horizontally. The angle of incidence (α) is set to 10° so that both the front and the rear airfoils operate close to their maximum aerodynamic performance point.[36] The local coordinates x_r and y_r are defined along the chordwise and chord-normal directions of the rear baseline and the rear serrated airfoils. Figure 3

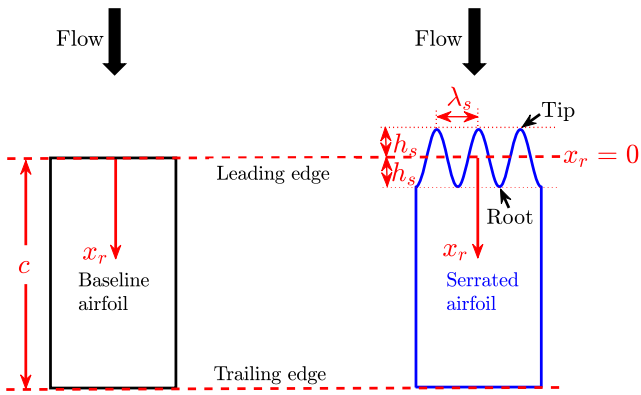

FIG. 3. Top-view showing a side-by-side comparison of the streamwise positions of the rear baseline airfoil with a straight leading edge and the rear serrated airfoil, the flow direction, and the geometrical parameters of the serration: wavelength λ_s = 9 mm and amplitude $2h_s$ = 15 mm. Both baseline and serrated airfoils have a chord length of c = 150 mm.

shows a side-by-side comparison between the baseline and serrated geometries of the rear airfoils used in the tandem arrangement. For consistency, $x_r = 0$ is defined at the leading edge of the rear baseline airfoil such that the tip and root of the rear serrated airfoil begin at $x_r = -0.05c$ and $0.05c$, respectively. The leading-edge serration has a wavelength $\lambda_s = 9$ mm and an amplitude (root-to-tip) $2h_s = 15$ mm, which has previously been shown to deliver notable noise reduction.[34]

C. Experimental approach

Far-field noise measurements are performed using an array of 20 microphones mounted on an arc above the test rig at regular angles from $\theta = 40^\circ$ to 135° in steps of 5° (see Fig. 1). The microphone array is made of 1/4-in. G.R.A.S. 40PL free-field microphones, which possess a large dynamic range with a maximum limit of 142 dB and cover the frequency range from 10 Hz to 20 000 Hz. The aerodynamic loading of the rear airfoil is investigated using pressure ports distributed along both the pressure and suction sides of the rear airfoil. There are in total 32 pressure ports, with 16 along each side, for both the baseline and serrated cases. The labeling of these pressure ports and their corresponding distances from the leading edge for the rear baseline and rear serrated airfoils are presented in Table I. In the case of the rear baseline airfoil [Table I(a)], the pressure ports have been distributed along the airfoil mid-plane on both the suction and pressure sides, while for the rear serrated airfoil, the ports have been distributed along the streamwise direction covering both the serration tip [Table I(b)] and root [Table I(c)] planes. It should be highlighted that the distribution, i.e., the distance from the leading edge, is identical on both sides of the airfoils; in addition, the tip and root planes share three common ports, namely, $P8_{s,t}$ ($P8_{s,r}$), $P9_{s,t}$ ($P9_{s,r}$), and $P10_{s,t}$ ($P10_{s,r}$), toward the trailing edge of the serrated airfoil. Due to the intrinsic complexity of the serration design, it is practically not possible to distribute the pressure port locations along a single serration root or tip plane to enable near-field correlation studies experimentally. However, the surface pressure fluctuations data, presented in Sec. III C, could serve as a validation case for future near-field correlation studies using computational fluid dynamics (CFD). Figure 4 shows a 3D computer-aided design (CAD) drawing of the baseline and serrated airfoils used to illustrate the locations and labeling of selected pressure ports on the suction side. Although only the suction side of the airfoils is visible in the figure, note that the pressure side bears exactly the same port distribution, i.e., both the locations and the labeling. The pressure ports are made from a 1.6 mm thick brass tube with a bore of diameter 0.4 mm and are flush-mounted perpendicular to the surface to avoid any kind of interference with the flow. The steady pressure data are acquired by a MicroDaq pressure scanner system at a sampling frequency of 1000 Hz for 60 s for both the baseline and serrated airfoils.

The unsteady surface pressure fluctuation (near-field) measurements are performed using remote-sensing probes via the same pressure ports as in the steady pressure measurement, as shown in Fig. 5(a). Each remote sensor consists of a microphone-holder assembly (Panasonic WM-61A microphones enclosed in a holder), connected using a transparent polyurethane tubing of 1.4 mm wall thickness and an inner and an outer diameter of 0.8 mm and 3.6 mm, respectively [see Fig. 5(b)]. In addition, a long termination tube is attached to the microphone-holder assemblies to avoid backward sound reflection and data contamination. All the remote-sensing microphones were calibrated with a reference G.R.A.S. 40PL microphone subjected to a white noise signal. The remote-sensing units are calibrated prior to the near-field measurements, so that any possible dampening of the amplitude of the pressure fluctuations due to the remote-sensing setup is accounted for in the calibration transfer function. The detailed calibration approach and description of the remote-sensing probe methodology can be found in Refs. 35 and 37. All unsteady surface pressure data are acquired simultaneously with the far-field noise measurements at a sampling frequency of 2^{16} Hz for 12s using two synchronized PXIe-4499 data acquisition cards mounted in a National Instruments PXIe-1062Q chassis. The power spectral density (PSD) is then calculated for all the far-field and the surface pressure fluctuation (near-field) data via Welch's method using a Hamming window with 50% overlap, resulting in

TABLE I. Labeling and the corresponding distance from the leading edge (x_r) of the pressure ports used for remote-sensing and surface pressure measurements on the rear baseline (a) and the rear serrated [(b) and (c)] airfoils. The labeling and locations of the pressure ports on the rear serrated airfoil's tip (b) and root (c) planes are shown separately. The port distribution shown in the table, i.e., the labeling and the distance from the leading edge, is identical on both the suction and pressure sides of the airfoils.

(a) Rear baseline airfoil

Port	P1	P2	P3	P4	P5	P6	P7	P8	P9	P10	P11	P12	P13	P14	P15	P16
x_r (mm)	2	5	8	11	17	23	29	35	44	53	62	71	80	89	107	116

(b) Rear serrated airfoil—Tip plane

Port	$P1_{s,t}$	$P2_{s,t}$	$P3_{s,t}$	$P4_{s,t}$	$P5_{s,t}$	$P6_{s,t}$	$P7_{s,t}$	$P8_{s,t}$	$P9_{s,t}$	$P10_{s,t}$
x_r (mm)	−3	0	5	9	19.5	34.5	54.5	73	93	113

(c) Rear serrated airfoil—Root plane

Port	$P11_{s,r}$	$P12_{s,r}$	$P13_{s,r}$	$P14_{s,r}$	$P15_{s,r}$	$P16_{s,r}$	$P8_{s,r}$	$P9_{s,r}$	$P10_{s,r}$
x_r (mm)	11.5	14.5	19.5	24.5	34.5	54.5	73	93	113

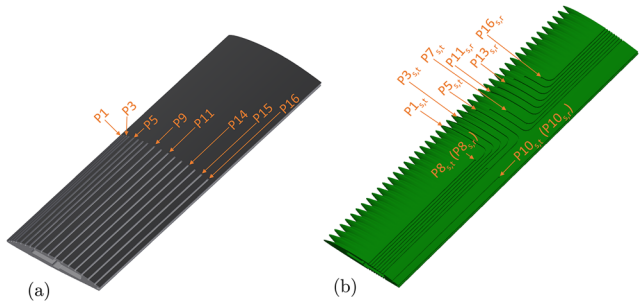

FIG. 4. Schematic showing the location of selected pressure ports on the (a) baseline and (b) serrated airfoils (flaps not shown). The distribution of the ports (location and labeling) on the pressure side is identical to that on the suction side displayed.

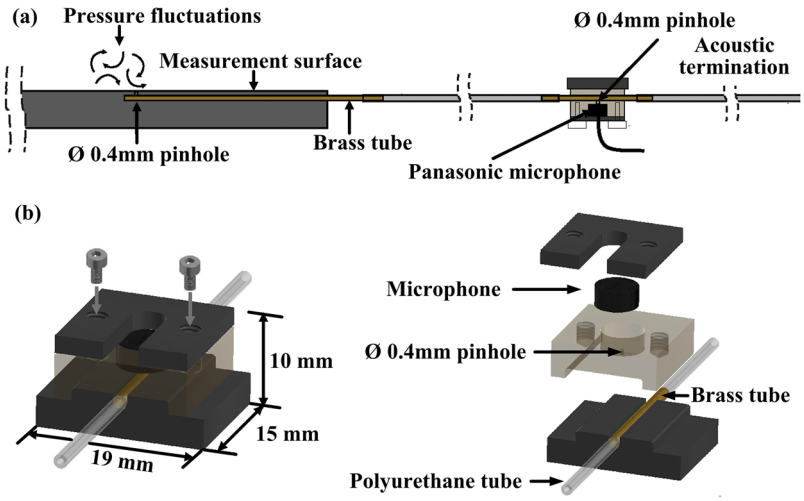

FIG. 5. Schematic of the remote-sensing probe configuration for the (a) full view of the airfoil and (b) assembly view and exploded view of the remote-sensing probe.

a final frequency spectral resolution of 2 Hz. All spectra presented are based on a reference sound pressure of 20×10^{-6} Pa.

The purpose of the present experiments is to examine the effectiveness of far-field noise reduction by using serrated leading edges on the rear airfoil in a tandem airfoil configuration. To achieve this, the data obtained with the rear airfoil with the serrated leading edge in a tandem configuration are compared against the data obtained with the one with a straight leading edge. Both the front and rear airfoils are set at an angle of incidence $\alpha = 10^{\circ}$, as shown in Fig. 2. The side-plate pair used to hold the rear airfoil is designed in such a way that it has the ability to slide continuously in a synchronized manner. This design has been used to measure the data at different rear airfoil vertical locations relative to the front airfoil. The chosen decent step-size is maintained at 2 mm, i.e., $\Delta W_y = 0.013c$. In order to better understand the aerodynamic performance and the near-field hydrodynamic characteristics of the serrated leading edge when the rear airfoil is being fully emerged inside the wake of the front airfoil, the experiments were carried out in two stages. In the first stage, the rear airfoil was carefully traversed vertically through the wake, as described earlier, and the corresponding far-field noise was measured. In the second stage, experiments on a selected number of vertical gap distances, with reference to the first stage, were performed to acquire steady and unsteady surface pressure measurements to provide physical explanation and insights into the observed trends in the far-field noise reductions.

III. RESULTS AND DISCUSSION

In this section, the far-field noise results for the tandem airfoil configuration, with and without the leading-edge serrations on the rear airfoil, see Fig. 1, will be presented. The far-field noise data will be provided for the tandem airfoil configuration, with the rear airfoil located over the range of vertical locations relative to the front airfoil (W_y). The results of far-field noise reduction due to application of the leading-edge serrations at various vertical locations (W_y) of the rear airfoil covering the entire wake as well as regions outside the wake of the front airfoil are first presented. From these results, two vertical locations (W_y) of the rear airfoil were identified for further detailed aeroacoustic and hydrodynamic analysis to better understand the noise-reduction mechanism and to shed light on how the root and tip regions of the leading-edge serrations contribute to the changes in the radiated far-field noise.

A. Far-field noise

Far-field noise measurements are taken with the airfoils set at an angle of incidence $\alpha = 10^{\circ}$ relative to the flow stream and gap distance $W_x/c = 0.3$, as shown in Fig. 2, in order to maximize the impact of the wake of the front airfoil on the rear one. Recall that the flow speed, U_0, is set to 25 m/s, which corresponds to the chord-based Reynolds number of $Re_c \approx 2.5 \times 10^5$. In order to investigate the interaction of the rear airfoil with different regions of the front airfoil wake flow field, the rear airfoil is installed on a sliding mechanism, enabling the vertical movement of the airfoil within $W_y/c = 0.16$–0.33, in $\delta W_y/c = 0.013$ steps of increments. The preliminary flow measurement analysis has shown that this vertical range is sufficient to fully capture the wake region, as well as the regions below and above the wake region.

Figure 6 shows a contour plot of ΔPSD due to the use of leading-edge serrations on the rear airfoil at various height positions (W_y) of the rear airfoil, where ΔPSD refers to the change in PSD between the tandem-baseline and tandem-serrated configurations: $\Delta\text{PSD} = \text{PSD}_{serrated} - \text{PSD}_{baseline}$. Thus, $\Delta\text{PSD} < 0$ denotes noise reduction and $\Delta\text{PSD} > 0$ denotes noise increase. The spectral plots in this paper hereafter are shown with respect to both the frequency, f (Hz), and the non-dimensional frequency, $kc = 2\pi fc/a$, where c is the chord length of the airfoils and a is the speed of sound under the present experimental condition. The data presented here are based on the far-field measurements at the polar angle of $\theta = 90^{\circ}$, at a distance of 1.75 m from the airfoils. As can be seen in Fig. 6, the resulting noise reduction (ΔPSD) reaches a maximum value within the vertical range of W_y tested, and the observed reduction fades as the rear airfoil is moved out of the front airfoil wake in either direction vertically. In the case of the rear baseline airfoil, i.e., with a straight leading edge, the gap turbulent flow interacts with the

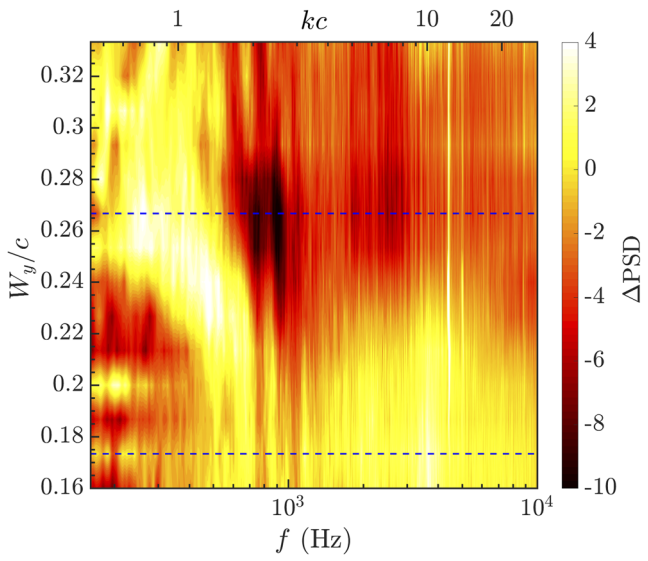

FIG. 6. Far-field noise reduction for the tandem airfoil configuration due to the use of serrations on the rear airfoil, measured using the $\theta = 90°$ microphone. The blue dashed lines show the two height locations (W_y) of the rear airfoil used for further detailed hydrodynamic analysis.

leading edge in a constructive way across the full span of the airfoil,[31] resulting in a significant noise radiation at low frequencies. In the case of the rear serrated airfoil, the noise radiation due to the turbulence impingement shows signs of significant noise reduction, which is believed to be partly due to destructive noise interferences, as explained in Refs. 19 and 26. The highest level of far-field noise reduction has been observed within the frequency range $kc \approx 1.5$–10, at the vertical gap distance of $W_y/c = 0.266$ ($W_y = 40$ mm), which is expected to correspond roughly to the central point of the front airfoil wake, i.e., the maximum velocity deficit point. Encouragingly, the use of leading-edge serrations on the rear airfoil can lead to up to 10 dB/Hz noise reduction where the rear airfoil interacts fully with the wake flow. The reduction of the interaction noise at frequencies $kc > 1.5$ is accompanied by a slight increase of up to 4 dB/Hz below $kc = 1$. The reason for this slight noise increase will be discussed later in Sec. III C. The results also show that when the rear airfoil is located below or above the front airfoil wake region, the value of ΔPSD reduces to nearly zero, indicating the absence of any wake flow interaction with the rear airfoil. Based on the results of ΔPSD presented here, two rear airfoil vertical locations, $W_y/c = 0.266$ (strong wake interaction) and $W_y/c = 0.173$ (insignificant wake interaction), have been identified (as shown by the blue dashed lines in Fig. 6) for further detailed hydrodynamic analysis in Secs. III B and III C.

Figure 7 provides a comparison of the far-field noise from the tandem-baseline and the tandem-serrated configurations. Figures 7(a) and 7(b) present, respectively, the results when the rear airfoil is located inside the front airfoil wake region ($W_y/c = 0.266$) and when it is outside the wake region ($W_y/c = 0.173$). The noise PSD data are presented for a far-field microphone at $\theta = 90°$, located at a distance of 1.75 m from the airfoils. The results of the isolated front airfoil and jet flow background noise are also provided for comparison. In the case of the rear airfoil located within the front airfoil wake region, as shown in Fig. 7(a), a clear broadband hump appears at around $0.7 < kc < 4$ in the case of tandem-baseline configuration, which is due to the interaction of the incoming turbulent wake flow with the rear airfoil, similar to that of the turbulence interaction noise identified by Gruber *et al.*[32] A comparison of the noise from tandem airfoil cases against that of the isolated front airfoil clearly shows the low-frequency noise amplification for frequencies up to $kc \approx 10$, due to the elevated noise level associated with the tandem airfoil configuration. The results also show clearly that the use of leading-edge serration on the rear airfoil can result in significant reduction of the radiated noise, by up to 12 dB/Hz, over the whole frequency spectrum. The use of leading-edge serration has also led to a slight shift of the far-field noise spectrum peak frequency $kc \approx 1.6$ from the baseline to a lower frequency of $kc \approx 1$ and a noise increase at lower frequencies ($kc \approx 0.6$–1.3) by up to 4 dB/Hz, which is considerably smaller than the reduction from $kc = 1.6$ onward. Figure 7(b) shows that as the rear airfoil is moved out of the wake region of the front airfoil, the distinct low-frequency broadband hump that arises inside the wake, as shown in Fig. 7(a), disappears and the PSD simply rolls off in a flat manner toward high

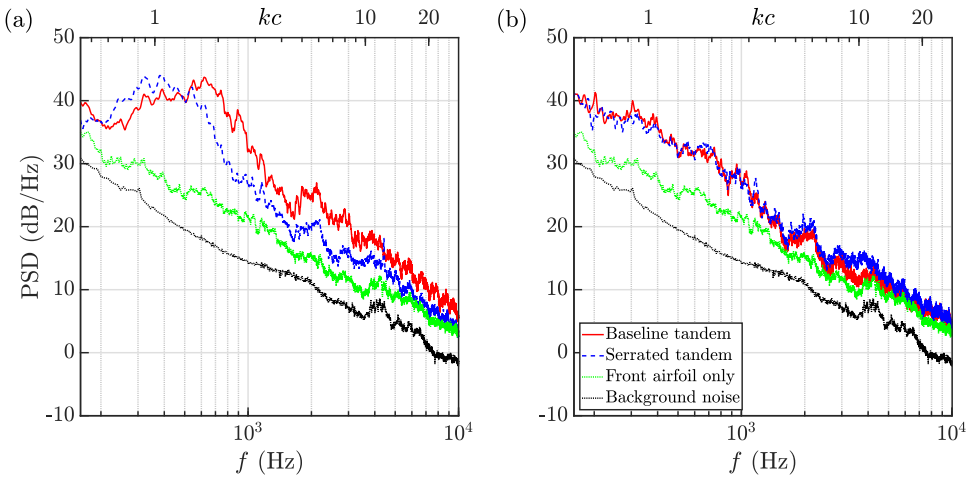

FIG. 7. Comparison of the $\theta = 90°$ far-field noise PSD for the tandem airfoil configuration at different rear airfoil vertical locations: (a) within the wake of the front airfoil, $W_y/c = 0.266$ ($W_y = 40$ mm); (b) outside the wake of the front airfoil, $W_y/c = 0.173$ ($W_y = 26$ mm).

frequencies. This reaffirms the observation earlier that the broadband hump is directly related to the interaction of the front airfoil wake flow with the rear airfoil. The results in Fig. 7(b) also show that the far-field noise spectra of the tandem-baseline and tandem-serrated configurations are very similar, indicating that in the absence of a strong turbulent wake flow interaction, the use of leading-edge serrations is ineffective. While the noise from the tandem airfoil configuration is generally higher than that of the isolated front airfoil case, by up to 5 dB/Hz, the lack of a distinct low-frequency hump and overall similarity of the spectra indicate that in the absence of a strong turbulent wake flow interaction, the dominant noise generation mechanism for the tandem configuration is the trailing-edge noise from the two airfoils.

Figure 8 shows the far-field noise directivity for the tandem-baseline and tandem-serrated configurations at selected frequencies, namely, kc = 0.7, 2.5, and 15. Based on the far-field noise data presented in Fig. 6, these frequencies correspond to, respectively, the low-frequency region ($0.45 < kc < 1.5$), where a slight noise increase has been observed, the frequency range with maximum noise reduction ($1.5 < kc < 8$), and the high-frequency region ($8 < kc < 27$), where no significant changes were observed. The background noise data, due to the noise from the jet and side plates, are also provided for comparison. The figures shown on the left, i.e., Figs. 8(a), 8(c), and 8(e), correspond to the case where the rear airfoil is inside the wake of the front airfoil ($W_y/c = 0.266$), and those to the right, i.e., Figs. 8(b), 8(d), and 8(f), correspond to the case where the rear airfoil is outside of it ($W_y/c = 0.173$). At $W_y/c = 0.266$, an increase in noise levels up to 4 dB/Hz has been noted in the low-frequency region (kc = 0.7), which is overridden by strong reduction levels up to 12 dB/Hz in the region of maximum attenuation ($kc = 2.5$), along with reductions up to 4 dB/Hz in the high-frequency region (kc = 15). The directivity of the noise generally assumes a dipole shape across all three kc presented, agreeing with the numerical study on turbulence–airfoil interaction noise by Polacsek *et al.*[16] On the other hand, outside the wake, there is a small noise reduction at $kc = 0.7$, whereas no significant change is observed at $kc = 2.5$. The results have also shown that the use of leading-edge serration on the rear airfoil does not change the directivity of the radiated noise regardless of whether the rear airfoil is located inside or outside of the front airfoil wake.

Figures 9(a) and 9(b) show the Overall Sound Pressure Level (OASPL) for the tandem-baseline and tandem-serrated configurations, obtained by integrating the PSD data over the frequency range 160 Hz–10 000 Hz for the cases W_y/c = 0.266 and W_y/c = 0.173, respectively. The jet flow background noise is also provided for comparison. As can be observed, in the case of the rear airfoil located inside the wake of the front airfoil ($W_y/c = 0.266$), the overall noise reduction is markedly evident with reduction levels in the 6 dB range in all directions, while when the rear airfoil is outside the wake of the front airfoil (W_y/c = 0.173), as seen in Fig. 9(b), the use of leading-edge serrations does not lead to any far-field noise reduction.

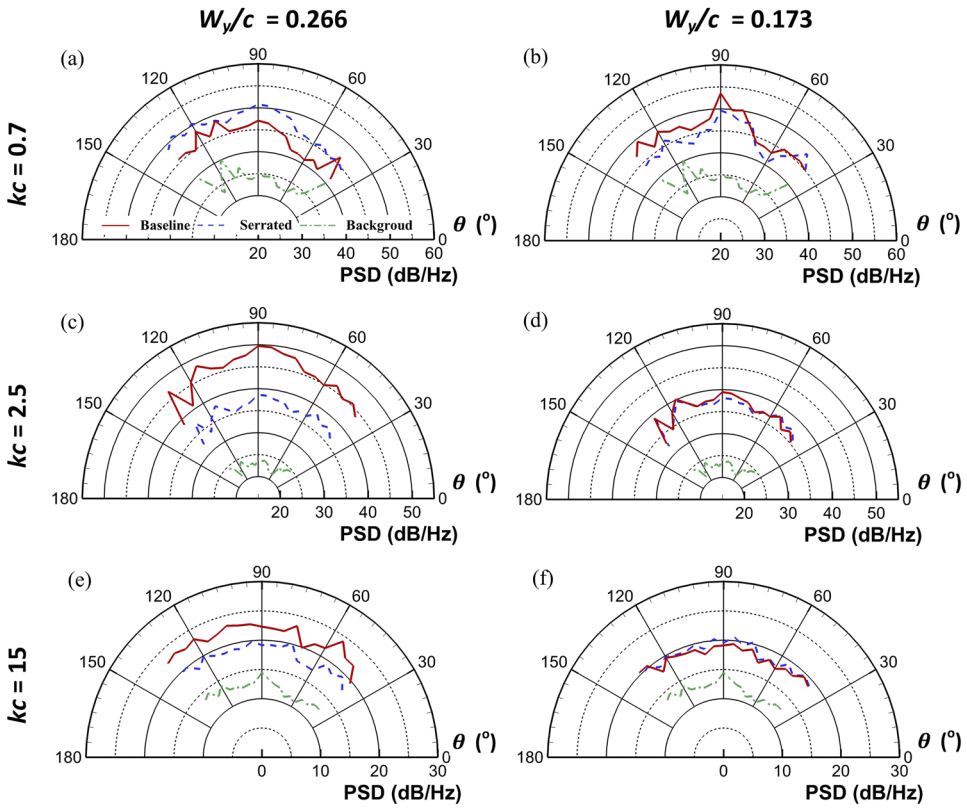

FIG. 8. Far-field noise directivity of the PSD (dB/Hz) plotted against θ for the background noise and the baseline and serrated tandem airfoil configurations for selected frequencies at different rear airfoil vertical locations: [(a), (c), and (e)] within the wake of the front airfoil (W_y/c = 0.266); [(b), (d), and (f)] outside the wake of the front airfoil (W_y/c = 0.173).

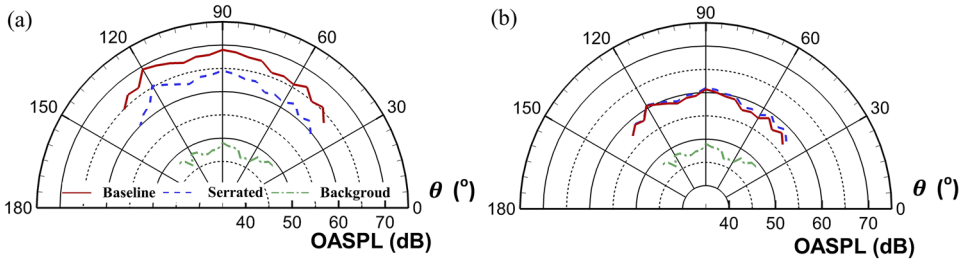

FIG. 9. Far-field noise directivity plots of the OASPL (dB) plotted against θ for the background noise and the baseline and serrated tandem airfoil configurations at different rear airfoil vertical locations: (a) within the wake of the front airfoil (W_y/c = 0.266); (b) outside the wake of the front airfoil (W_y/c = 0.173).

B. Aerodynamic loading

The changes in the aerodynamic loading of the rear airfoil in a tandem configuration, caused by the application of leading-edge serrations, are investigated locally at different regions of the airfoil, i.e., near the leading edge, the mid-chord, and the trailing edge, using static and root-mean-square pressure distribution. Note that the focus of these measurements is not to calculate aerodynamic lift and drag, but to better understand the modifications to the static pressure distribution and its fluctuation caused by the leading-edge serrations. The mean (C_p) and root-mean-square ($C_{p_{rms}}$) pressure coefficients of the rear airfoils in tandem-baseline and tandem-serrated configurations at $\alpha = 10^\circ$ and gap distances $W_x/c = 0.3$ and $W_y/c = 0.266$ are presented in Figs. 10(a) and 10(b), respectively. This case corresponds to a vertical location at which the rear airfoil is inside the wake of the front airfoil. The most obvious difference between the tandem-baseline and the tandem-serrated static pressure distribution occurs close to the leading edge of the rear airfoil along the suction surface. While the baseline airfoil experiences a constant increase in C_p, the leading-edge serrated airfoil initially

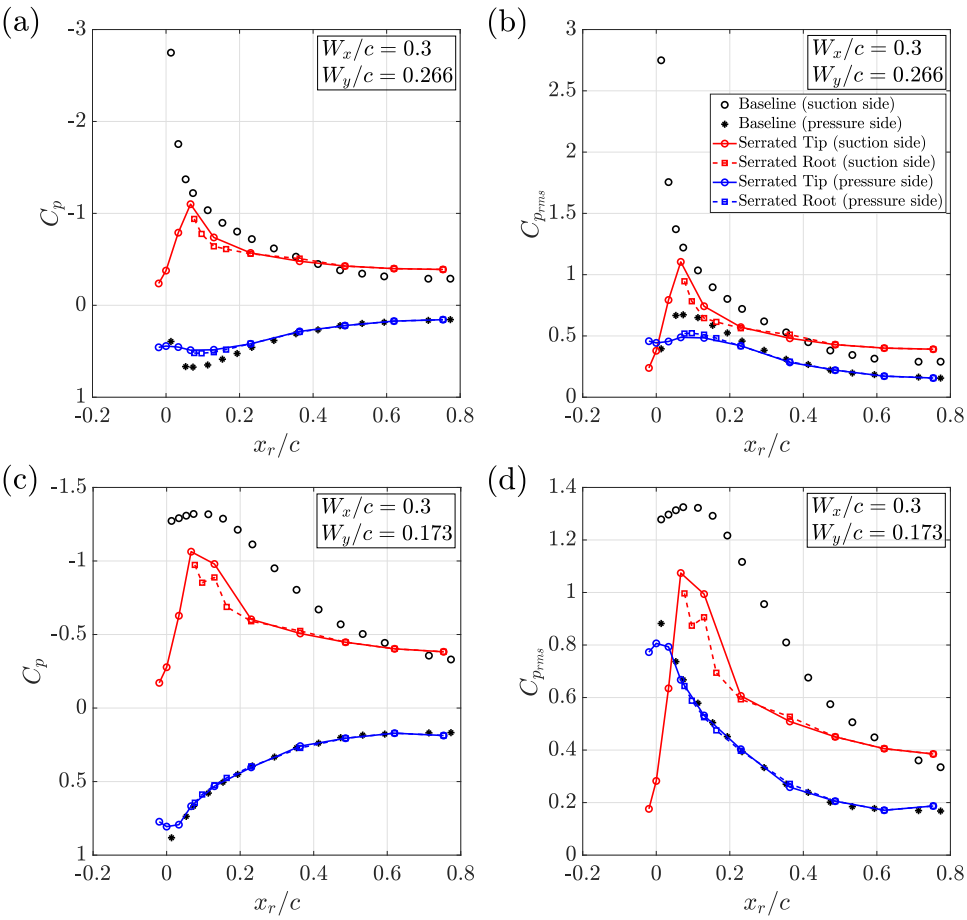

FIG. 10. Mean pressure (C_p) and the root-mean-square pressure ($C_{p_{rms}}$) distribution over the rear airfoil with the axial and vertical gap distances of [(a) and (b)] W_x/c = 0.3 and W_y/c = 0.266 and [(c) and (d)] W_x/c = 0.3 and W_y/c = 0.173.

undergoes a rapid drop in C_p from a relatively higher value as compared to the baseline. This sudden change close to the leading-edge region of the serrated airfoil has also been observed by Clair *et al.*[17] in their study of leading-edge serrated airfoils. Both the serration root and tip planes retain a higher C_p value than the baseline airfoil for $x_r/c < 0.4$. On the pressure (lower) surface, both the serration tip and root planes show a decrease in C_p for a small region near the leading edge ($x_r/c < 0.25$), after which no difference is noted compared to the baseline case. As can be seen in Fig. 10(a), the C_p curves on the pressure and suction sides shrink closer together for the rear serrated airfoil compared to the rear baseline one. Although extracting lift and drag information from C_p data alone for three-dimensional airfoils, especially with the serrated leading edge, is not trivial, the C_p curves shrinking closer together might imply a reduced lift for the rear serrated airfoil compared to the rear baseline one, consistent with findings from lift–drag measurements performed in earlier works.[19,38]

The root-mean-square pressure ($C_{p_{rms}}$) can provide an insight into the time-averaged unsteady loading exerted on the airfoil. As can be seen in Fig. 10(b), the fluctuating pressure coefficient ($C_{p_{rms}}$) is reduced significantly on the serration tip and root planes compared to the baseline from the leading-edge to the mid-chord location, i.e., $x_r/c \approx 0.4$, on both the suction and pressure sides, which suggests a substantial reduction in the time-averaged pressure fluctuation, i.e., the overall unsteady loading, on the rear serrated airfoil compared to the rear baseline airfoil. For the region $x_r/c > 0.4$, the serration tip and root planes exhibit a small increase in the unsteady loading on the suction side while showing no change on the pressure side when compared to the baseline case.

The mean (C_p) and root-mean-square ($C_{p_{rms}}$) pressure coefficients at $W_y/c = 0.173$ are presented in Figs. 10(c) and 10(d), respectively. This case corresponds to a location of the rear airfoil outside the wake of the front airfoil, which means the rear airfoil is subjected to primarily a much less turbulent, but significantly deflected flow. As discussed in Sec. III A, in this region, the two airfoils are expected to have noise radiation from their trailing-edge regions as for both airfoils, the incoming flow is non-turbulent. As can be seen in Fig. 10(c), on the suction side, an increase in C_p can be observed for both the serration tip and root planes compared to the baseline case over the leading-edge and mid-chord regions, i.e., $x_r/c < 0.6$. On the pressure side, C_p distribution for both the serration tip and root planes is similar to the baseline case, except for a small region near the leading edge and the trailing edge. Hence, with reference to the C_p results at $W_y/c = 0.266$, it can be confirmed that the use of leading-edge serration is able to alter the aerodynamic loading close to the leading edge notably along the suction side, but the effect remains limited along the pressure side. The unsteady pressure loading $C_{p_{rms}}$, on the other hand, is observed to be reduced on both the serration tip and root planes compared to the baseline case over the leading-edge and mid-chord regions, i.e., $x_r/c < 0.6$, on the suction side of the airfoil and yet the serrations do not have much effect on the unsteady loading experienced by the pressure side of the airfoil.

Clearly, similar to the static pressure coefficient, the pressure fluctuation $C_{p_{rms}}$ is reduced considerably with the leading-edge serrations applied to the rear airfoil. More importantly, unlike C_p, reduction in $C_{p_{rms}}$ can be observed for both the suction and pressure sides when the rear airfoil is immersed inside of the front airfoil wake. However, $C_{p_{rms}}$ only provides the time-averaged information of the unsteady loading acting on the airfoil. In order to further understand the exact changes in the energy–frequency content of the flow near the airfoil surface, the unsteady surface pressure fluctuation will be examined in Sec. III C.

C. Unsteady surface pressure

The unsteady surface pressure fluctuations have been investigated to better understand the unsteady aerodynamic loading and the associated energy–frequency content acting on the rear airfoil as a direct result of its interaction with the front airfoil wake. In this section, we present and analyze the changes that the leading-edge serration brings forward in terms of the frequency-dependent unsteady aerodynamic loading. This can also help in enhancing the understanding of the effects of leading-edge serration when being subjected to the laminar or turbulent incoming flow. Furthermore, these measurements provide valuable information to explain the trends observed in far-field noise measurements. The unsteady surface pressure measurement locations are provided in Table I, and details are explained in Sec. II B.

Figure 11 shows the surface pressure PSD data from selected ports over the rear airfoil. In this case, the rear airfoil is located inside the wake of the front airfoil, i.e., $W_x = 0.3c$ and $W_y = 0.266c$. The figures to the left, i.e., Figs. 11(a), 11(c), and 11(e), show the surface pressure fluctuation PSD (near-field) data on the suction (top) side and the figures to the right, i.e., Figs. 11(b), 11(d), and 11(f), show the near-field data on the pressure (bottom) side for the baseline and serrated-tip and serrated-root planes, respectively. For the baseline case, on the suction side [Fig. 11(a)], the surface pressure energy content gradually decreases from the leading-edge region to the trailing-edge region with the increasing distance from the leading edge. This is an indication that the unsteady loading exerted on the airfoil is primarily due to the incoming turbulent flow. This is in clear contrast to the cases when the incoming flow is laminar, i.e., the exerted unsteady loading is mainly due to the boundary layer and it increases from the leading edge to the trailing edge as will be seen later. In addition, as can be seen, there appears to be a small kink in the surface pressure fluctuation PSD profiles for all the port locations shown, i.e., P1 ($x_r/c = 0.113$) to P13 ($x_r/c = 0.533$) for frequencies $kc \approx 2.75$–5.5 (1000 Hz–2000 Hz). The kink could be due to the transition from the turbulence interaction dominated spectrum to the boundary-layer hydrodynamics dominated spectrum.

The unsteady loading on the pressure side of the airfoil [Fig. 11(b)] in the case when the airfoil is inside the front airfoil wake flow field behaves in a similar way to that on the suction side, though with lower PSD levels. One can, therefore, conclude that in the case of the baseline airfoil (straight leading edge), interacting with the turbulent incoming flow, the unsteady loading on both the suction and pressure sides of the leading-edge area has the largest contribution to the overall unsteady loading of the airfoil. The serrated airfoils behave in a very different way due to the way their leading edge responds to the interaction with the impinging turbulence. The tip plane of the rear serrated airfoil exhibits a fundamentally different behavior possibly due to the emergence of counter-rotating vortices from the tip (tip flow), as previously observed through particle image velocimetry (PIV) measurements.[39,40] The serration tip

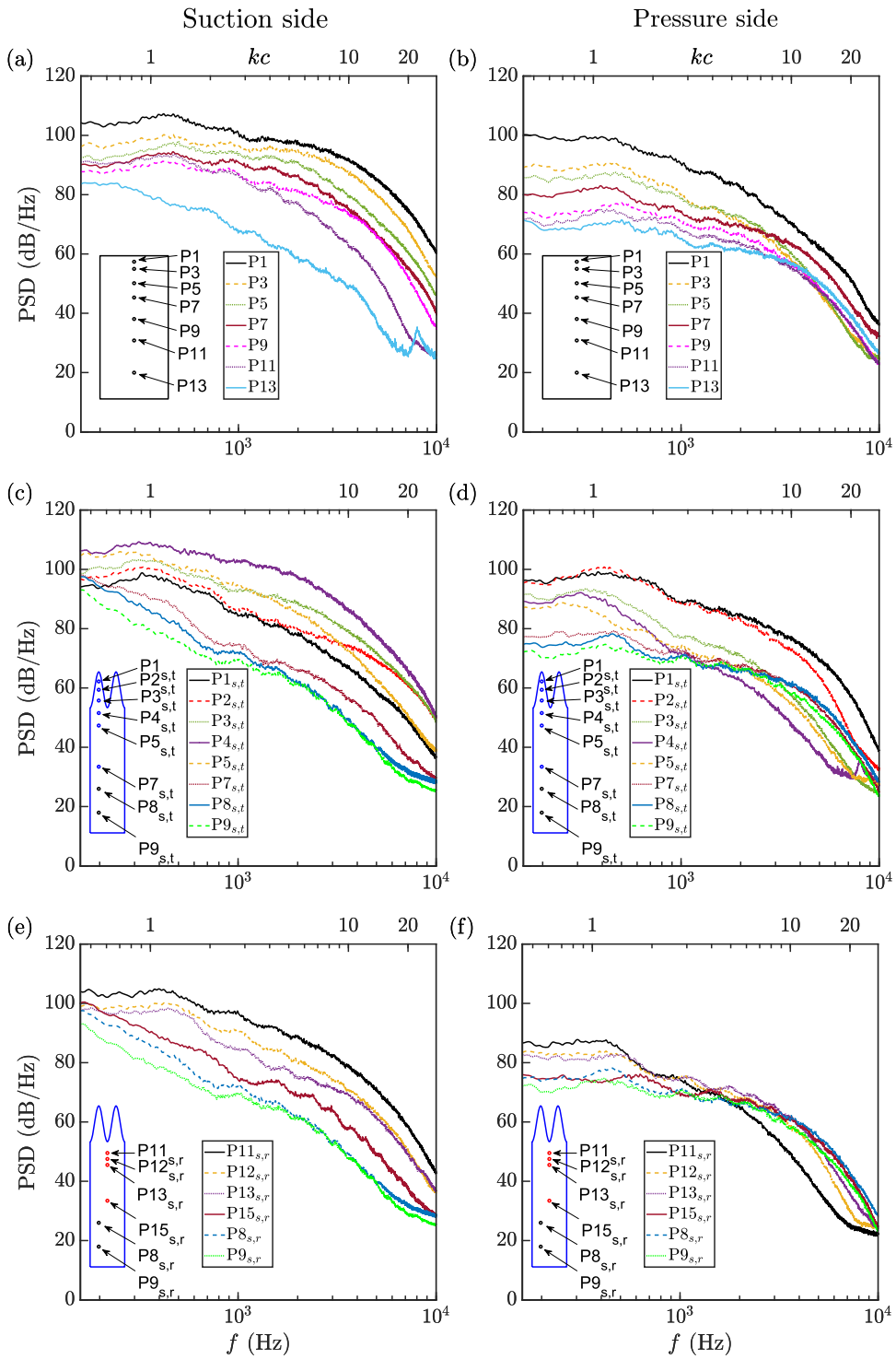

FIG. 11. Near-field unsteady surface pressure data on the rear airfoil from selected remote-sensing ports at W_x/c = 0.3 and W_y/c = 0.266 for (a) the baseline case (suction side); (b) the baseline case (pressure side); (c) the serration tip plane (suction side); (d) the serration tip plane (pressure side); (e) the serration root plane (suction side); and (f) the serration root plane (pressure side). Ports P8 and P9 are common ports for the serration root and tip planes.

plane measures the impact of the separated flow from the leading edge until a certain point downstream because of the appearance of counter-rotating vortices. As a result, the energy is seen to initially increase from $P1_{s,t}$ to $P4_{s,t}$, i.e., $-0.02 < x_r/c < 0.06$, on the suction side [Fig. 11(c)], and from $P1_{s,t}$ to $P2_{s,t}$, i.e., $-0.02 < x_r/c < 0$, on the pressure side [Fig. 11(d)], before decreasing toward the trailing edge. Along the root plane, unlike the tip plane, the source strength is not reduced compared to the baseline case, as noted by Kim *et al.*[18]

As a result, the flow exhibits quite a similar variation to the baseline case on the suction [Fig. 11(e)] and the pressure [Fig. 11(f)] sides, i.e., a consistent decrease in the energy–frequency content from the leading edge to the trailing edge. The surface pressure energy levels on the pressure side, in general, are smaller than those on the suction side for all, *i.e.*, baseline, serrated-tip, and serrated-root profiles, meaning that the flow over the suction side is likely to contribute more significantly to the radiated far-field noise. Moreover, a closer examination on the individual PSD curve reveals that there appears to be a small, but still noticeable broadband hump from $kc = 0.8$ to 4 for the rear baseline airfoil on both the suction and pressure sides, which corresponds very well to the broadband hump observed from the far-field measurements in Fig. 7 earlier. Moving to the rear serrated airfoil, the broadband hump diminishes slightly, though it remains visible. At this point of time, it is difficult to verify if a small frequency shift can be observed in the surface pressure fluctuation of the rear serrated airfoil, similar to that of the far-field noise results, which will be elucidated further in the following discussion.

The corresponding surface pressure fluctuation PSD data for the case where the rear airfoil is outside the wake of the front airfoil, i.e., $W_x/c = 0.3$ and $W_y/c = 0.173$, are shown in Fig. 12. On the suction side [Fig. 12(a)], the PSD profiles initially exhibit an increase from the leading edge to about 12% of the chord, from P1 ($x_r/c = 0.013$) to P5 ($x_r/c = 0.113$), before reducing until the trailing edge. On the pressure side [Fig. 12(b)], the PSD envelope exhibits a gradual decrease in the energy–frequency content from the leading edge to the trailing edge while maintaining the profile pattern. The PSD profiles themselves, however, are clearly different from the corresponding baseline case when the rear airfoil is located inside the front airfoil wake, with a clear peak seen across the entire airfoil between approximately $kc \approx 2$ and 3 (800 Hz–900 Hz). Furthermore, for the tip plane of the leading-edge serrated airfoil seen in Fig. 12(c), the PSD profiles increase initially from $P1_{s,t}$($x_r/c = -0.02$) to $P4_{s,t}$ ($x_r/c = 0.06$) before decreasing on the suction side, whereas on the pressure side [Fig. 12(d)], they decrease all the way from the leading edge to the trailing edge. On the pressure side, the serration tip plane [Fig. 12(d)] behaves similar to the baseline case [Fig. 12(b)] exhibiting a distinct peak, but the peak is shifted slightly toward lower frequencies, $kc \approx 1.5$–2 (700 Hz–750 Hz). The serration root plane on the suction side [Fig. 12(e)] exhibits a gradual decrease in surface pressure energy across the entire airfoil. The pressure side [Fig. 12(f)], unlike the suction side [Fig. 12(e)], has a broadband hump in the surface pressure fluctuation PSD profiles [Fig. 12(f)], which decay from $P12_{s,r}$ ($x_r/c = 0.097$) to $P8_{s,r}$ ($x_r/c = 0.49$), before increasing slightly from $P8_{s,r}$ ($x_r/c = 0.49$) to $P9_{s,r}$ ($x_r/c = 0.62$). However, recall that no apparent broadband hump is observed in the far-field noise results in this case (i.e., outside of the wake), and it corroborates with the argument earlier that when the rear airfoil is positioned outside of the front airfoil wake, the far-field noise is dominated by the trailing-edge noise of the tandem airfoils. With the knowledge of the surface pressure fluctuation PSD from leading to trailing edges, it will be useful to compare the individual behavior of the PSD profiles between the baseline, serrated-tip, and serrated-root profiles at similar chordwise locations.

A comparison of the surface pressure fluctuation PSD between the rear baseline (straight leading edge) and the rear serrated airfoils in the tandem configuration for $W_y/c = 0.266$ (inside of the front airfoil wake) is presented in Fig. 13. Note that the pressure ports are chosen such that their chordwise distances to their respective leading edge are comparable with each other, as indicated in Fig. 13. First of all, a comparison of the PSD profiles of the baseline port P1 ($x_r/c = 0.113$) and serration tip plane ports $P1_{s,t}$ ($x_r/c = -0.02$) and $P2_{s,t}$ ($x_r/c = 0$) on the suction side is shown in Fig. 13(a). As can be seen, the noise reduction near the leading edge due to the serration tip plane is considerably effective over the entire frequency range, with reduction levels reaching as high as 20 dB/Hz. A comparison of the ports $P1_{s,t}$ and $P2_{s,t}$ shows that the exerted surface pressure energy does not change greatly over the serration region, particularly at low frequencies, namely, $kc < 5.5$ (less than 2000 Hz). For frequencies $kc > 5.5$, the observed reduction further increases sharply, immediately downstream of the serration tip, i.e., going from $P1_{s,t}$ to $P2_{s,t}$, as shown in Fig. 13(a). On the pressure side [Fig. 13(b)], the PSD levels for the baseline and serration tip plane remain comparable until about $kc \approx 4.2$ (1500 Hz), after which the serration tip plane exhibits a small increase compared to the baseline case. It is worthwhile to mention that from the individual profiles in Figs. 13(a) and 13(b), a frequency shift of the broadband hump to the lower frequencies can indeed be seen for the serrated-tip plane as compared to the baseline, with a significant reduction in the PSD levels. In contrast, the serrated-root plane shows little changes in terms of both the broadband peak frequency and magnitude of the surface pressure fluctuation. Moving downstream where the serrated-root plane emerges in the comparison, Figs. 13(c) and 13(d) show the comparison of the exerted energy surface pressure PSD, i.e., the unsteady loading, on the suction and the pressure side, respectively, between the baseline and serration tip and root planes, at about $x/c = 0.1$. This location also corresponds to roughly the end of the serration on the tip plane and immediately downstream of the airfoil leading edge along the root plane. On the suction side [Fig. 13(c)], the surface pressure measurements along the tip and root planes both show an increase at low frequencies, up to about $kc \approx 1.6$ (600 Hz) and $kc \approx 3.2$ (1200 Hz), respectively, compared to the baseline case, followed by ~8 dB/Hz–10 dB/Hz reduction at higher frequencies. On the pressure side [Fig. 13(d)], both the serration tip and root planes exhibit unsteady loading reduction, except for an increase in the low-frequency region up to about $kc \approx 1$ (350 Hz) for the tip plane. In addition, when compared to the corresponding baseline case, the serrated-root plane achieves more reduction in surface pressure energy than the serrated-tip plane on the suction side, while it is the opposite on the pressure side. Finally, Figs. 13(e) and 13(f) show the comparison of the exerted unsteady loading at about $x_r/c = 0.35$. On the suction side [Fig. 13(e)], the PSD profiles follow the similar trend as in Fig. 13(c), i.e., a small increase near the leading edge, up to $kc \approx 1$ (350 Hz) along the root and tip planes, before obtaining a strong reduction in the unsteady loading all the way to the trailing edge. However, at this distance from the leading edge, i.e., nearly mid-chord, both the root and tip planes show a very similar surface pressure fluctuation PSD, indicating that the tip and root flows have merged and formed a more uniform flow field. On the pressure side [Fig. 13(f)], both the serration root and tip planes cause a minor increase in the surface pressure energy.

The use of leading-edge serrations, while reducing the broadband hump in the far-field noise spectra arising from the turbulence interaction, tends to have a shift in the energy contents toward lower

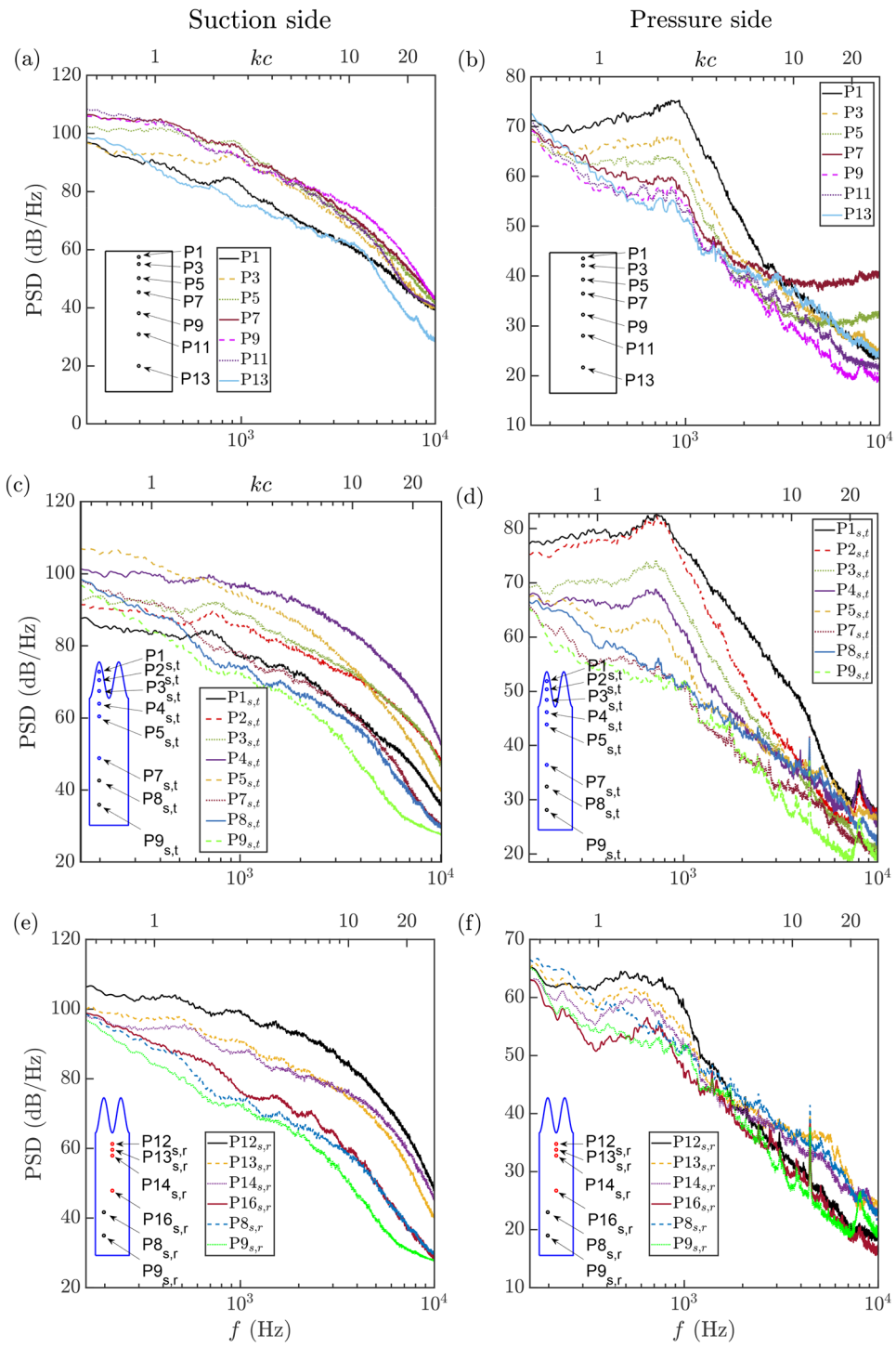

FIG. 12. Near-field unsteady surface pressure data on the rear airfoil from selected remote-sensing ports at W_x/c = 0.3 and W_y/c = 0.173 for (a) the baseline case (suction side); (b) the baseline case (pressure side); (c) the serration tip plane (suction side); (d) the serration tip plane (pressure side); (e) the serration root plane (suction side); and (f) the serration root plane (pressure side). Ports P8 and P9 are common ports for the serration root and tip planes.

frequencies, which manifests as a small noise increase in the low frequency region when the rear airfoil is inside the wake of the front airfoil, as observed previously in Fig. 7 (Sec. III A). The near-field measurements reveal the same shift toward low-frequency regions in both serration tip and root planes near the leading-edge and mid-chord regions, consistent with the far-field noise spectra shift. For instance, the baseline airfoil has a hump centered around $kc \approx 1.2$ (425 Hz), while the tip plane of the serrated airfoil has the hump

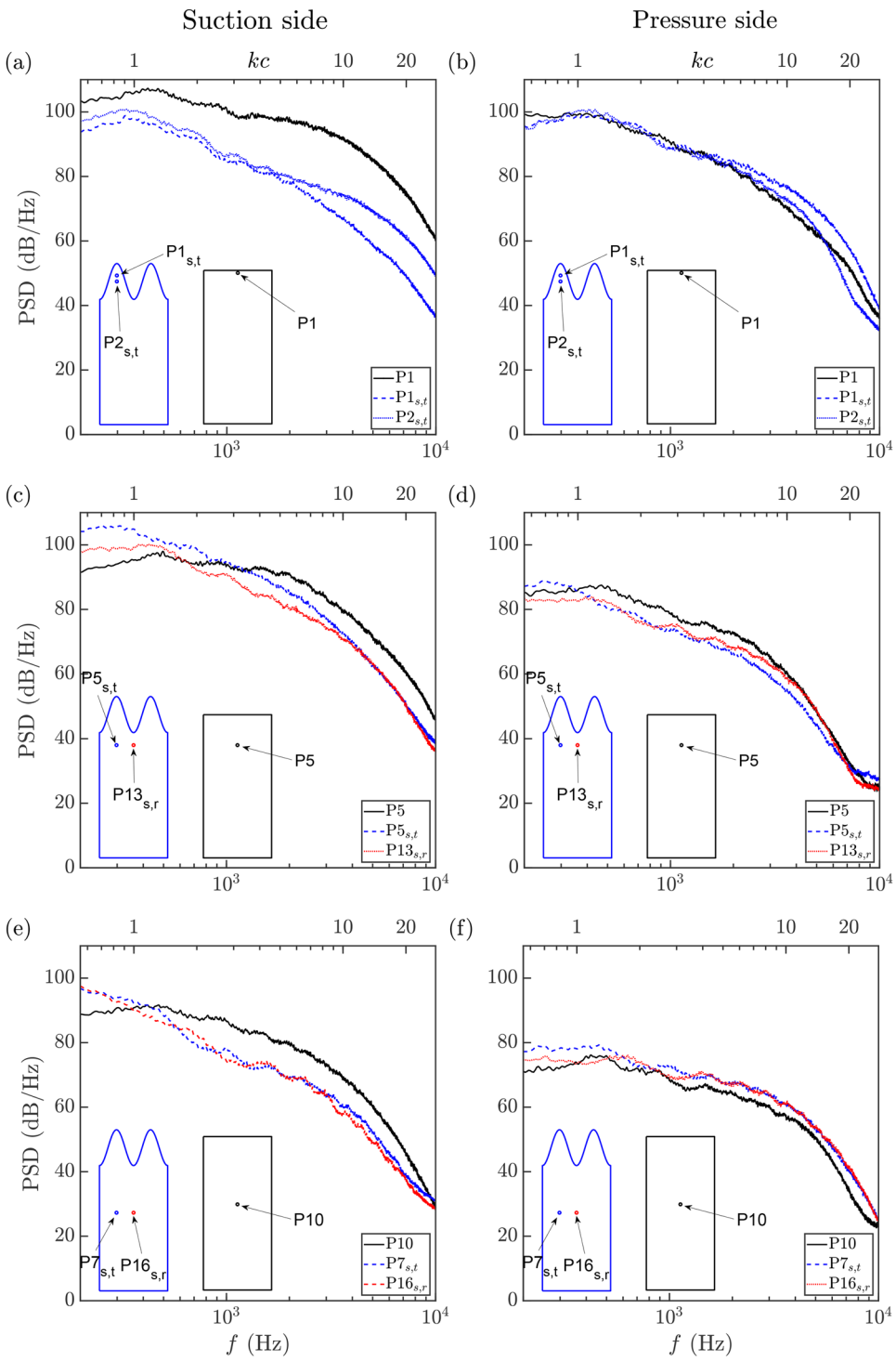

FIG. 13. Comparison of the near-field unsteady surface pressure data on the rear airfoil between the baseline and serrated configurations from selected remote-sensing ports at W_x/c = 0.3 and W_y/c = 0.266. Results are presented for the chordwise locations of [(a) and (b)] x_r/c = 0; [(c) and (d)] x_r/c = 0.13; and [(e) and (f)] x_r/c = 0.363. The figure schematically shows the location of the data ports presented, which are also listed in Table I.

centered around $kc \approx 0.9$ (350 Hz) near the leading edge [Fig. 13(a)]. Similarly, the frequency shift is also observed along the root plane of the serrated airfoil [Figs. 13(c) and 13(d)]. The shift toward low frequencies due to serration is accompanied by an increase in PSD of the surface pressure fluctuations on both the suction and pressure sides [Figs. 13(c)–13(f)], although the PSD increase along the pressure side is less notable than that along the suction side. Moreover, the tip plane along the mid-chord region contributes most to

the observed increase in far-field noise PSD in the low-frequency region (Fig. 7) when the rear airfoil is inside the front airfoil wake. Thus, it can be inferred that the turbulence interaction noise between the front airfoil wake and the leading edge of the rear airfoil is proportional to the unsteady loading on the surface near the rear airfoil leading-edge regions. Moreover, as the reduction in the near-field surface pressure energy content is primarily concentrated around the leading-edge regions on the suction side, it can be

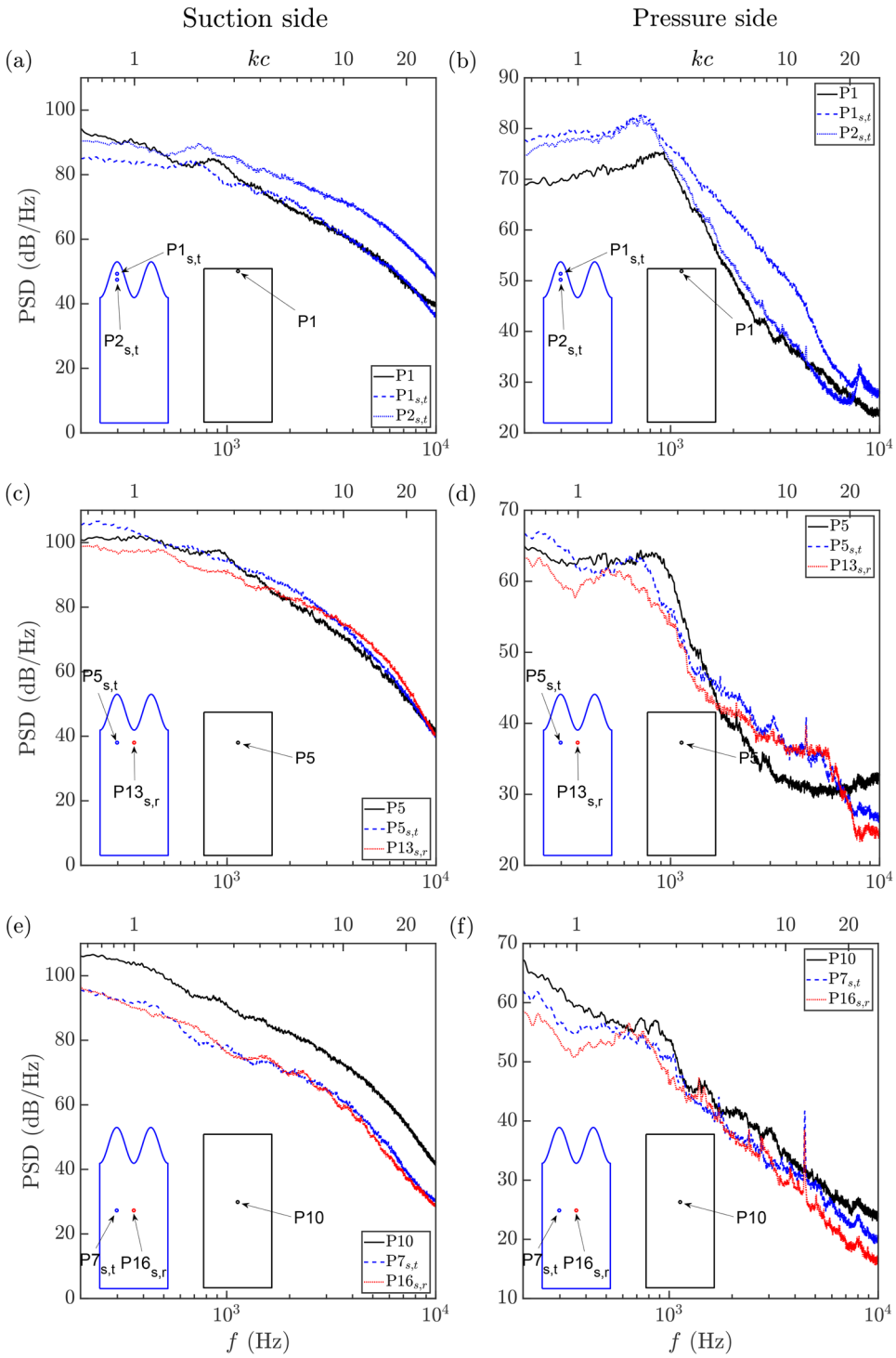

FIG. 14. Comparison of the near-field unsteady surface pressure data on the rear airfoil between the baseline and serrated configurations from selected remote-sensing ports at W_x/c = 0.3 and W_y/c = 0.173. Results are presented for the chordwise locations of [(a) and (b)] x_r/c = 0; [(c) and (d)] x_r/c = 0.13; and [(e) and (f)] x_r/c = 0.363. The figure schematically shows the location of the data ports presented, which are also listed in Table I.

concluded from the present results that the suction side of the rear airfoil close to the leading-edge region is primarily responsible for the observed far-field turbulence interaction noise between the front airfoil wake and the rear airfoil. According to the analytical findings from Lyu and Azarpeyvand[31] and Chaitanya *et al.*,[19] the leading-edge serration effectively reduces scattered noise through destructive interference along the incoherent spanwise sources. In the present experiments, it has also been demonstrated that in addition to the destructive interference, the modification of the flow characteristics by the leading-edge serrations could also lead to a significant reduction in the unsteady surface loading on the rear airfoil, which in turn causes a reduction in the turbulence interaction noise.

To complete the discussion, Fig. 14 shows a similar comparison for the $W_y = 0.173c$ case, i.e., the case when the rear airfoil is located outside the wake of the front airfoil. On the suction side near the leading edge [Fig. 14(a)], the serrated case displays an initial increase in surface pressure energy. In this case, the rear airfoil has been moved out of the wake of the front airfoil, and as a result, the two airfoils will act as two independent sources of self-noise, as discussed earlier in Sec. III A. Near the leading edge, the serration tip port $P1_{s,t}$ ($x_r/c = -0.02$) shows a decrease in PSD compared to the baseline case P1 ($x_r/c = 0.013$), but only in the low frequency region, i.e., $kc < 3.6$ ($f < 1300$ Hz). Then, within the tip plane near the leading edge, i.e., going from $P1_{s,t}$ ($x_r/c = -0.02$) to $P2_{s,t}$ ($x_r/c = 0$), an increase in PSD is observed. This is because the ports $P1_{s,t}$ and $P2_{s,t}$ are nearest to the leading edge along the tip plane, and hence, $P1_{s,t}$ and $P2_{s,t}$ are well inside the chordwise point, where the tip flow will cease to have its effect. On the pressure side near the leading edge [Fig. 14(b)], contrary to what was seen in the corresponding inside-wake case [Fig. 13(b)], PSD levels increase up to 6 dB/Hz at all frequencies. The PSD profile for the baseline case also has a broadband frequency hump and a distinct peak of $kc = 2.6$ (950 Hz). The use of the leading-edge serrated rear airfoil keeps the structure of the PSD profile, but the energy peak shifts to lower frequency $kc \approx 2$ (750 Hz), suggesting that the frequency shift could be present regardless of the incoming flow turbulence level, as a natural flow modification by the serration geometry. As shown in Fig. 14(c), going downstream along the chord, i.e., at about $x_r/c = 0.1$, the PSD profiles of the serration tip, $P5_{s,t}$ ($x_r/c = 0.13$), and root, $P13_{s,r}$ ($x_r/c = 0.13$), planes initially show reduction in surface pressure energy until about $kc \approx 1.6$ (600 Hz) and $kc \approx 3.2$ (1200 Hz), respectively, before showing an increase compared to the corresponding baseline, P5 ($x_r/c = 0.113$), on the suction side. On the pressure side [Fig. 14(d)], there is noise reduction for both serration root and tip ports (except a small increase for the serration tip) until $kc \approx 4.1$ (1500 Hz) and $kc \approx 4.4$ (1600 Hz), respectively, after which the surface pressure PSD level increase happens again. The surface pressure PSD level increasing at higher frequencies could be a result of the superfluous noise that the serrated leading edges are known to produce at high frequencies.[41] In general, the root plane is observed to cause more surface pressure PSD level reduction than the tip plane. Moving further downstream closer to the trailing edge, at about $x_r/c = 0.35$, the reduction in the PSD levels due to use of serrations becomes clearly evident on both suction [Fig. 14(e)] and pressure [Fig. 14(f)] sides across almost the entire frequency spectrum with fairly comparable reduction contributions from the root and the tip planes.

IV. CONCLUSIONS

In propulsion systems involving multiple rows of blades, the interaction of the blades' gap flow with downstream blades can be a major source of noise. In the present study, the effects of applying leading-edge serration on the rear airfoil in a tandem airfoil configuration have been investigated experimentally as a viable passive noise mitigation strategy to reduce turbulence interaction noise. From the far-field noise measurements, a clear broadband hump in the noise spectra arises due to the turbulence interacting with the leading edge when the rear airfoil is fully immersed in the wake of the front airfoil and the hump disappears as it moved out of the wake. More importantly, the far-field noise measurements show a significant reduction in the turbulence interaction noise when leading-edge serrations are applied to the rear airfoil. On the other hand, when the leading-edge serrations are applied to the rear airfoil placed outside the wake of the front airfoil, no far-field noise reduction has been observed. Furthermore, the directivity study from the far-field microphone arc on either discrete frequencies or the integrated overall sound pressure level indicates that the noise directivity remains comparable between the tandem-baseline (straight leading edge on the rear airfoil) and tandem-serrated cases, with the directivity being essentially dipolar.

The static pressure coefficients and unsteady surface pressure fluctuation data have also been measured to understand the changes in the aerodynamic loading caused by the application of leading-edge serrations and the respective contribution of the serrated-tip and serrated-root planes to the observed reduction in the radiated far-field noise as well as to provide further physical insight into the noise-reduction mechanism. From the root-mean-square of the static surface pressure coefficient ($C_{p_{rms}}$) distribution, it is evident that the use of leading-edge serrations causes a notable drop in the time-averaged fluctuation on the static surface pressure on both the suction and pressure sides of the rear airfoil, in particular, close to the leading-edge region of $x_r/c < 0.2$. A closer examination on the profiles of the surface pressure fluctuation PSD reveals that a broadband hump, similar to those observed in the far-field noise spectra, exists in both the rear baseline and rear serrated airfoils on the suction side, close to the leading-edge regions. Compared to the rear baseline case, the peak of the broadband hump appears to shift toward lower frequencies. The significant resemblance between the near-field surface pressure fluctuation and the far-field radiated noise, together with a reduction of up to 20 dB/Hz in the near-field surface pressure PSD levels through the use of leading-edge serration, indicates that first, the surface pressure fluctuation on the suction side of the rear airfoil close to the leading-edge region is an important contributor to the turbulence interaction noise in the tandem airfoil configuration. Second, the use of leading-edge serration on the rear airfoil proves to be effective in reducing the unsteady loading, i.e., the energy–frequency content of the surface pressure fluctuation, on the rear airfoil over a wide range of frequencies, thus leading directly to the notable reduction in far-field noise. In addition to the destructive interference demonstrated in the literature, the modification to the dynamics of the flow and the unsteady loading could also play a crucial role in the effectiveness of leading-edge serration to achieve noise reduction. Last but not least, it should be mentioned that toward the mid-chord region, the serrated-root plane contributes more effectively to the reduction in the unsteady

airfoil loading than the serrated-tip plane, although both are to a much less extent than the leading-edge regions.

ACKNOWLEDGMENTS

The first author (SH.S.V.) would like to acknowledge the financial support of the University of Bristol EPSRC Doctoral Prize Scheme via Grant No. EP/R0254251. The third author (B.Z.) would like to acknowledge the financial support of EPSRC via Grant No. EP/R010846/1.

DATA AVAILABILITY

The data that support the findings of this study are available from the corresponding author upon reasonable request.

REFERENCES

[1]WHO, "Environmental noise guidelines for the European region," World Health Organization Regional Office for Europe, Denmark, 2018, ISBN 978 92 890 5356 3.
[2]T. Brooks, D. Pope, and M. Marcolini, "Airfoil self-noise and prediction," NASA-RP-1218, 1989.
[3]X. Liu, H. Kamliya Jawahar, M. Azarpeyvand, and R. Theunissen, "Aerodynamic performance and wake development of airfoils with serrated trailing-edges," AIAA J. **55**, 3669–3680 (2017).
[4]A. Finez, M. Jacob, E. Jondeau, and M. Roger, "Broadband noise reduction with trailing edge brushes," AIAA Paper 2010-3980, 2010.
[5]S. A. Showkat Ali, M. Azarpeyvand, and C. R. Ilário da Silva, "Trailing-edge flow and noise control using porous treatments," J. Fluid Mech. **850**, 83–119 (2018).
[6]Q. Ai, M. Azarpeyvand, X. Lachenal, and P. M. Weaver, "Aerodynamic and aeroacoustic performance of airfoils with morphing structures," Wind Energy **19**(7), 1325–1339 (2016).
[7]B. Arnold, T. Lutz, E. Krämer, and C. Rautmann, "Wind-turbine trailing-edge noise reduction by means of boundary-layer suction," AIAA J. **56**, 1843–1854 (2018).
[8]M. Szőke and M. Azarpeyvand, "Active flow control methods for the reduction of trailing edge noise," AIAA Paper 2017-3004, 2017.
[9]R. K. Amiet, "Acoustic radiation from an airfoil in a turbulent stream," J. Sound Vib. **41**, 407–420 (1975).
[10]P. Migliore and S. Oerlemans, "Wind tunnel aeroacoustic tests of six airfoils for use on small wind turbines," J. Sol. Energy Eng. **126**, 974–985 (2004).
[11]F. E. Fish and J. M. Battle, "Hydrodynamic design of the humpback whale flipper," J. Morphol. **225**, 51–60 (1995).
[12]T. Bachmann, S. Klän, W. Baumgartner, M. Klaas, W. Schröder, and H. Wagner, "Morphometric characterisation of wing feathers of the barn owl *Tyto alba* pratincola and the pigeon *Columba livia*," Front. Zool. **4**, 23 (2007).
[13]H. S. Yoon, P. A. Hung, J. H. Jung, and M. C. Kim, "Effect of the wavy leading edge on hydrodynamic characteristics for flow around low aspect ratio wing," Comput. Fluids **49**, 276–289 (2011).
[14]P. T. Soderman, "Leading edge serrations which reduce the noise of low-speed rotors," NASA Technical Note, Report No. NASA TN D-7371, 1973.
[15]A. S. Hersh, P. T. Soderman, and R. E. Hayden, "Investigation of acoustic effects of leading-edge serrations on airfoils," J. Aircr. **11**, 197–202 (1974).
[16]C. Polacsek, V. Clair, G. Reboul, and H. Deniau, "Turbulence-airfoil interaction noise reduction using wavy leading edge: An experimental and numerical study," in *Proceedings of the Inter-Noise, Osaka, Japan, 4–7 September 2011* (Institute of Noise Control Engineering/Japan & Acoustical Society of Japan, 2011), pp. 170–180.
[17]V. Clair, C. Polacsek, T. Le Garrec, G. Reboul, M. Gruber, and P. Joseph, "Experimental and numerical investigation of turbulence-airfoil noise reduction using wavy edges," AIAA J. **51**, 2695–2713 (2013).
[18]J. W. Kim, S. Haeri, and P. F. Joseph, "On the reduction of aerofoil-turbulence interaction noise associated with wavy leading edges," J. Fluid Mech. **792**, 526–552 (2016).
[19]P. Chaitanya, P. Joseph, S. Narayanan, C. Vanderwel, J. Turner, J. W. Kim, and B. Ganapathisubramani, "Performance and mechanism of sinusoidal leading edge serrations for the reduction of turbulence-aerofoil interaction noise," J. Fluid Mech. **818**, 435–464 (2017).
[20]X. Huang, "Theoretical model of acoustic scattering from a flat plate with serrations," J. Fluid Mech. **819**, 228–257 (2017).
[21]J. M. Turner and J. W. Kim, "On the universal trends in the noise reduction due to wavy leading edges in aerofoil-vortex interaction," J. Fluid Mech. **871**, 186–211 (2019).
[22]L. J. Ayton and J. W. Kim, "An analytic solution for the noise generated by gust-aerofoil interaction for plates with serrated leading edges," J. Fluid Mech. **853**, 515–536 (2018).
[23]S. Narayanan, P. Joseph, S. Haeri, and J. W. Kim, "Noise reduction studies from the leading edge of serrated flat plates," AIAA Paper 2014-2320, 2014.
[24]T. M. Biedermann, P. Czeckay, T. F. Geyer, F. Kameier, and C. O. Paschereit, "Effect of inflow conditions on the noise reduction through leading edge serrations," AIAA J. **57**, 4104–4109 (2019).
[25]T. Geyer, S. Wasala, and E. Sarradj, "Experimental study of airfoil leading edge combs for turbulence interaction noise reduction," Acoustics **2**, 207–223 (2020).
[26]P. Chaitanya, P. Joseph, S. Narayanan, and J. W. Kim, "Aerofoil broadband noise reductions through double-wavelength leading-edge serrations: A new control concept," J. Fluid Mech. **855**, 131–151 (2018).
[27]C. C. Paruchuri, S. Narayanan, P. Joseph, and J. W. Kim, "Leading edge serration geometries for significantly enhanced leading edge noise reductions," AIAA Paper 2016-2736, 2016.
[28]P. Chaitanya, P. Joseph, and L. J. Ayton, "Leading-edge profiles for the reduction of airfoil interaction noise," AIAA J. **58**, 1118–1129 (2020).
[29]L. J. Ayton and P. Chaitanya, "An analytical and experimental investigation of aerofoil-turbulence interaction noise for plates with spanwise-varying leading edges," J. Fluid Mech. **865**, 137–168 (2019).
[30]A. S. H. Lau, S. Haeri, and J. W. Kim, "The effect of wavy leading edges on aerofoil-gust interaction noise," J. Sound Vib. **332**, 6234–6253 (2013).
[31]B. Lyu and M. Azarpeyvand, "On the noise prediction for serrated leading edges," J. Fluid Mech. **826**, 205–234 (2017); arXiv:1706.04509.
[32]M. Gruber, P. Joseph, C. Polacsek, and T. P. Chong, "Noise reduction using combined trailing edge and leading edge serrations in a tandem airfoil experiment," AIAA Paper 2012-2134, 2012.
[33]Y. D. Mayer, H. K. Jawahar, M. Szőke, S. A. S. Ali, and M. Azarpeyvand, "Design and performance of an aeroacoustic wind tunnel facility at the University of Bristol," Appl. Acoust. **155**, 358–370 (2019).
[34]S. Vemuri, X. Liu, B. Zang, and M. Azarpeyvand, "Leading-edge serrations for noise control from tandem airfoil configuration," AIAA Paper 2019-2556, 2019.
[35]X. Liu, S. A. Showkat Ali, and M. Azarpeyvand, "On the application of trailing-edge serrations for noise control from tandem airfoil configuration," AIAA Paper 2017-3716, 2017.
[36]X. Liu, "Aerodynamic and wake development of aerofoils with trailing-edge serrations," Ph.D. thesis, University of Bristol, 2018.
[37]Y. Mayer, B. Zang, and M. Azarpeyvand, "Aeroacoustic characteristics of a NACA 0012 airfoil for attached and stalled flow conditions," AIAA Paper 2019-2530, 2019.
[38]K. L. Hansen, R. M. Kelso, and B. B. Dally, "Performance variations of leading-edge tubercles for distinct airfoil profiles," AIAA J. **49**, 185–194 (2011).
[39]F. Avallone, S. Pröbsting, and D. Ragni, "Three-dimensional flow field over a trailing-edge serration and implications on broadband noise," Phys. Fluids **28**, 117101 (2016).
[40]G. Bampanis, M. Roger, D. Ragni, F. Avallone, and C. Teruna, "Airfoil-turbulence interaction noise source identification and its reduction by means of leading edge serrations," AIAA Paper 2019-2741, 2019.
[41]T. P. Chong, T. Biedermann, O. Koster, and S. M. Hasheminejad, "On the effect of leading edge serrations on aerofoil noise production," AIAA Paper 2018-3289, 2018.